ELSEVIER

Ceramics International 33 (2007) 107–114

CERAMICS INTERNATIONAL

www.elsevier.com/locate/ceramint

Influence of texture on electrical properties of ZnO ceramics prepared by extrusion and spark plasma sintering

Jiang Li Ning [a,*], Da Ming Jiang [a], Kyoung Hun Kim [b], Kwang Bo Shim [b]

[a] *Analysis and Measurement Center, School of Materials Science and Engineering, Harbin Institute of Technology, Harbin 150001, China*

[b] *Department of Ceramic Engineering, Ceramic Processing Research Center, Hanyang University, Seoul 133-791, Korea*

Received 7 June 2005; received in revised form 26 June 2005; accepted 22 August 2005
Available online 21 October 2005

Abstract

An extrusion-spark plasma sintering (SPS) process was successfully utilized to obtain a textured, near full dense homogeneous bulk ZnO ceramics. Rod-like, anisotropic ZnO particles were extruded and sintered, and highly *c*-axis-preferred orientation was obtained in the bulk ZnO, which can be called as fiber texture. The textured bulk ZnO showed more low-angle grain boundaries compared with that without texture. It was found that the highly preferred orientation decreased the electrical resistivity obviously in the bulk ZnO at room temperature. The observed high proportion of low-angle grain boundaries due to the texture resulted in a quite lower resistivity in grain boundaries at room temperature, which was the main reason for the reduction in electrical resistivity of the textured bulk ZnO ceramics.

Keywords: A. Extrusion; C. Electrical properties; D. ZnO; Texture

1. Introduction

Zinc oxide is an n-type semiconductor and is a multifunctional material with wide range of applications such as thermoelectrics [1,2], varistors, gas sensors, piezoelectrics, electrodes for solar cells [3], and optoelectronic devices [4,5].

Single crystal of ZnO has a wurtzite-type hexagonal structure. In addition, many researches have confirmed that ZnO single crystals exhibit highly anisotropic properties [6–9]. For example, Nakamura et al. [6] stated that the electrical resistivity of the single crystal was 3 Ω cm through *a*-axis, whereas it was ~8.2 Ω cm through *c*-axis at room temperature.

In thin film applications, this anisotropy has been successfully utilized by texturing ZnO films to enhance performance of the devices. Highly *c*-axis-oriented ZnO thin films were obtained using various methods such as sol–gel process [7–9], radio frequency sputtering [10], metalorganic vapor-phase epitaxy (MOVPE) [11], and chemical spray pyrolysis [12]. Thin films of ZnO with the *c*-axis orientation perpendicular to the substrate show piezoelectric properties and are useful in surface acoustic wave devices (SAW), bulk acoustic wave devices (BAW), acoustic-optic devices, and microelectromechanical systems (MEMS) [7,9,13]. Besides, Ohyama et al. [8] reported that highly preferred orientation was effective in reducing the film resistivity in ZnO films, because of the shorter carrier path length in a *c*-plane and the reduction in the scattering of the carriers at the grain boundaries and crystal defects, which increases the apparent carrier mobility. Bao et al. [9] and Schuler et al. [14] also reported the same effect of the highly preferential orientation on reducing the electrical resistivity of ZnO films.

But compared to films, there are only a very few studies on texture development in the form of bulk ZnO ceramics [15,16]. Eda et al. [17] and Suvaci et al. [16] stated that the application of the bulk ZnO ceramics as varistors could benefit from texturing. Isobe et al. [15] showed that texturing enhanced the thermoelectric performance of yttrium-substituted $(ZnO)_5In_2O_3$ elec-

* Corresponding author. Tel.: +86 451 13304609164/86417617; fax: +86 451 86414234.
E-mail addresses: haowen20012003@yahoo.com.cn, haowen20012003@hotmail.com (J.L. Ning).

0272-8842/$30.00
doi:10.1016/j.ceramint.2005.08.005

troceramics. Therefore, if bulk polycrystalline ZnO ceramics are textured and exhibit single crystal-like anisotropic properties, the properties will be greatly enhanced in certain crystallographic directions.

Extrusion was confirmed to be an effective process in aligning the whisker-shaped ceramic particles with organic binder in order to obtain an unidirectionally oriented microstructure after sintering [18–21].

The spark plasma sintering (SPS) process is a type of pressure-sintering method with rapid-heating, low-sintering-temperature, and short-sintering-period characteristics. SPS process uses high temperature spark plasma generated by discharging the gaps between powder particles with on–off electrical energy and joule heating from the graphite mold by an electrical current. The generation of the spark plasma in the initial stage of the SPS process accelerates the neck formation and thermal diffusion and performs a surface-activating and cleaning effect on the particles being sintered. Also, the electrical field formed by the dc current accelerates diffusion. SPS process makes it possible to form a homogeneous microstructure with fine grains, because an excessive or abnormal grain growth can be prohibited by sintering at low temperature and within short time. Also, clean grain boundaries can be formed due to the surface-cleaning effect in SPS process, for the generated spark discharge and/or plasma is able to clean the surfaces from adsorbed species, such as CO_2, H_2O, and OH [22,23]. With these merits, SPS process has been widely utilized for the preparation of electroceramics in recent years.

In the present study, one kind of rod-like anisotropic ZnO particle was selected as the original powder, and an extrusion-SPS process was performed in order to get a highly preferred orientation in the bulk polycrystalline ZnO ceramics. As the electrical resistivity of bulk ZnO ceramics is concerned in various applications such as thermoelectrics, gas sensors, varistors and so on, the influence of texture on the electrical resistivity of bulk ZnO was studied in this research.

2. Experimental procedure

Commercially available ZnO (High-purity Chemical, >99.9 wt%, Korea) particles were used as starting materials, which were shaped rod-like and anisotropic.

The dough used for extrusion was prepared by mixing the ZnO powder with 10 wt% polyethylene ethanol (PVA) as the binder, 3 wt% glycerine as the plasticizer and 2 wt% liquid paraffin as the lubricant, and kneaded by roll mixer.

Fig. 1 shows the schematic illustration of the extrusion procedure. First, the dough was removed into the chamber of the extrusion instrument. Then, pressure was put on the dough through the piston by a hydraulic press. The tube of the extrusion instrument was rectangular in shape, and the orifice was 12 mm wide and 0.5 mm high. The green sheets were extruded out through the nozzle with the same dimensions as the orifice. The green sheets were dried at room temperature in a closed chamber to prevent any contamination from environment. After drying, the green sheets were stacked one by one following the extrusion direction, as shown in Fig. 1.

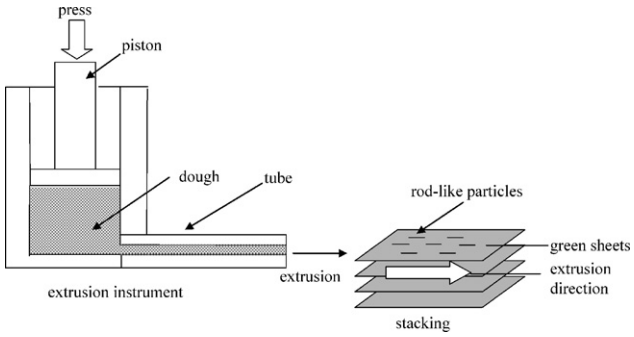

Fig. 1. Schematic illustration of the extrusion procedure and the stacking of the green sheets following the extrusion direction.

Then, the stacked sheets were cut into round pieces with 10 mm diameter forming a cylinder without destroying the alignment of the particles in each piece. The cylinder was removed to a graphite mold used for spark plasma sintering, as shown in Fig. 2(a). The extrusion direction of the particles was marked on the mold for further processing of the sintered sample. After burning out the organic binder in open air, the graphite mold was mounted inside an SPS system (SPS-515s, Sumitomo Coal Mining Co., Japan). After applying an initial pressure of 50 MPa, a two-stage heating-rate sintering was performed. From room temperature to 700 °C, 30 °C/min was performed, while from 700 to 1000 °C, 100 °C/min was performed. It was sintered for 3 min at 1000 °C and then cooled at a rate of 50 °C/min. After finishing the sintering process, the pressure was relaxed. During the sintering process, N_2 gas was flowing through the SPS chamber for protection. The sintered body was typically 10 mm in diameter and 4 mm in thickness. Then, the sintered sample was cut perpendicular to the extrusion direction for microstructure analysis, as shown in Fig. 2(b). Therefore, there were two surfaces of the sintered sample on which the microstructure was examined. One was the surface perpendicular to the SPS pressure direction, which will be called *surface a* in the following part of this paper, and the other was the surface perpendicular to the extrusion direction, which will be called *surface c* correspondingly, as shown in Fig. 2(b). Another spark plasma-sintered ZnO sample with the same particles without extrusion was also prepared in the same way for comparison.

Archimedes' method was used to measure the density of the sintered samples. The microstructures of the ZnO powder and the SPS samples were examined in a scanning electron microscope (SEM, JSM-5900LV, JEOL) and a transmission electron microscope (TEM, 200CX, JEOL). XRD patterns of the ZnO particles were measured by an X-ray diffractometer (XRD, D/max-2C, Rigaku Denki) with Cu Kα radiation. The grain orientation and grain boundary characteristics were evaluated by SEM-EBSD (electron back scattered diffraction, Inca Crystal, Oxford instruments, UK) system. Impedance spectra were measured at room temperature by an impedance analyzer (Precision Component Analyzer 6440A, Wayne Kerr). The frequency range of the measurements was from 20 Hz to 3 MHz. The measurements of impedance spectra were in the axial direction of the cylindrical samples. Electrodes were

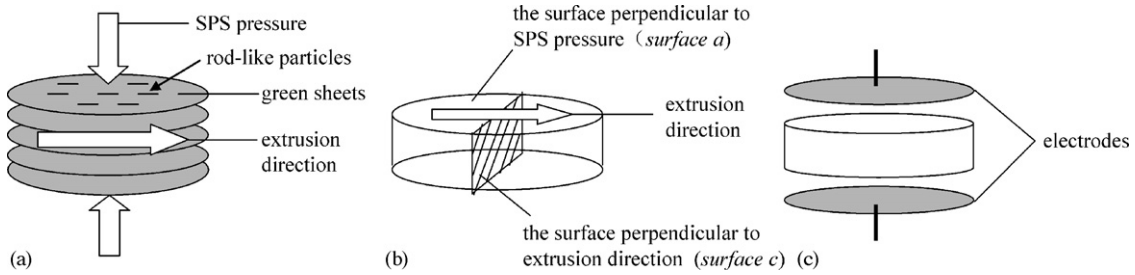

Fig. 2. Schematic illustrations of sample preparation: (a) removing the cylinder of stacked green sheets into the graphite mold; (b) cutting the sintered sample perpendicularly to the extrusion direction for microstructure analysis; (c) preparing electrodes by Pt-paste coating.

prepared by coating Pt-paste on both of the surfaces perpendicular to SPS pressure (*surface a*) as shown in Fig. 2(c).

3. Results and discussion

3.1. Particle characteristics and alignment by extrusion

Fig. 3 shows the SEM micrograph of the commercial ZnO particles. It can be seen that the morphology of the particles was rod-like. The size and the shape of the particles were identical. The size was ~1 μm in long axes and 0.2 μm in short axes, so the aspect ratio of the particles was ~5. The orientation of the particles was analyzed by TEM diffraction. The result is shown in Fig. 4, in which the arrowhead points to the long axial direction of the rod-like particle. From the diffraction pattern, it can be deduced that the particle was elongated along the [0 0 0 1] direction (i.e., *c*-axis direction) of the ZnO hexagonal lattice.

In order to obtain the identical alignment of the rod-like anisotropic ZnO particles, the extrusion method was utilized. After the extrusion, the long axes of the rod-like particles would be aligned along the extrusion direction identically. This alignment is achieved by the rotation of the rod-like particles when flowing through the tube of the extrusion instrument with the organic binder during extrusion. When the dough is flowing through the tube during extrusion, the shear stress developed between the inner walls of the tube makes the long axes of the rod-like particles rotate to the extrusion direction, and finally the alignment of the particles is obtained [19]. Since the long axial direction was the *c*-axis direction of the ZnO particles, therefore, the *c*-axes of the ZnO particles would be all aligned along the extrusion direction after the extrusion process.

Fig. 5 shows the XRD patterns of the un-extruded powder and the extruded green sheet with binder burned out and diffracted from the top surface of the green sheet. It can be seen that after extrusion the intensity of the (0 0 0 2) peak decreased a lot, and the intensities of the $(1\,0\,\bar{1}\,0)$ and $(1\,1\,\bar{2}\,0)$ (i.e., the two prismatic planes) peaks increased compared with those of the un-extruded particles. So it can be concluded that the prismatic planes of the ZnO particles were aligned in a direction perpendicular to the extrusion direction, and the *c*-axes of the particles were in a direction parallel to the green sheet surface after the extrusion process. It meant that the extrusion process was effective for the rotation of the rod-like anisotropic ZnO particles. It was also confirmed that the long axial direction of the particles was [0 0 0 1] indeed.

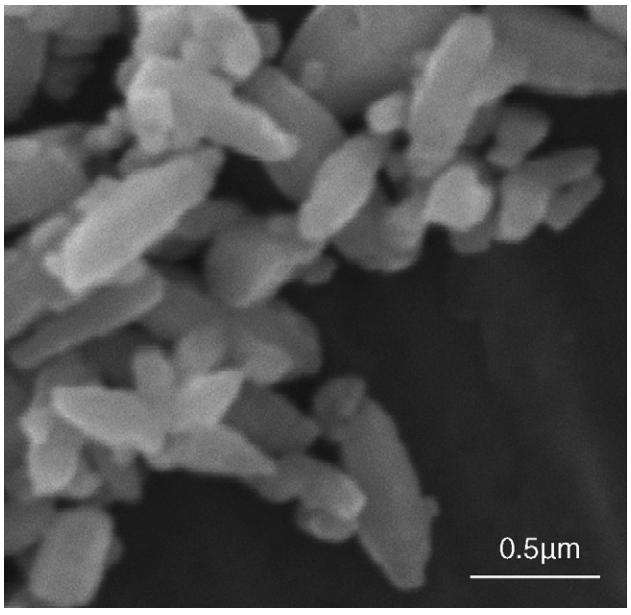

Fig. 3. SEM image of the commercial ZnO powder.

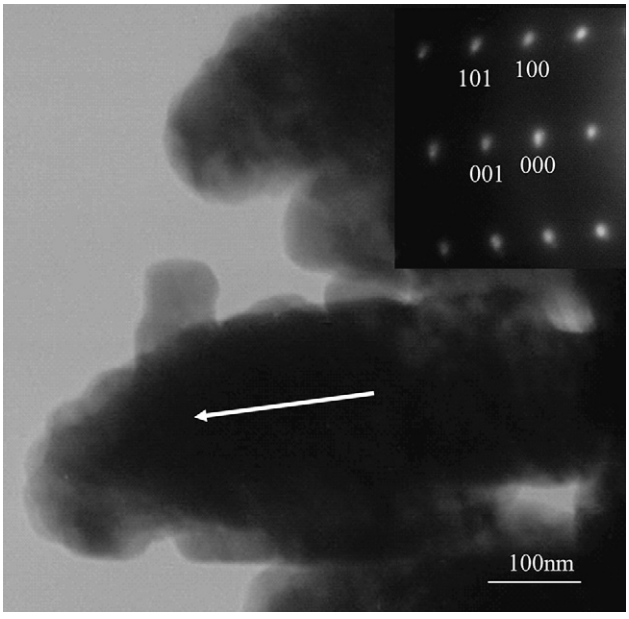

Fig. 4. TEM image and diffraction pattern of the commercial ZnO powder.

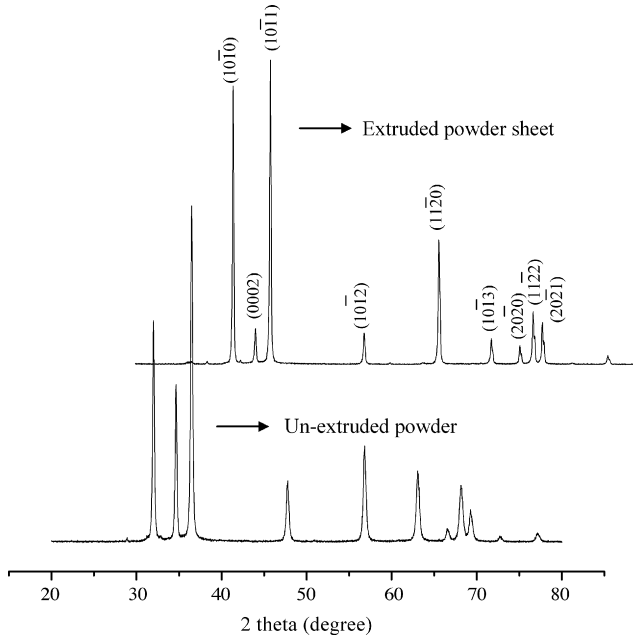

Fig. 5. XRD patterns of the un-extruded powder and the extruded powder sheet with binder burned out.

3.2. Spark plasma sintering

After drying, stacking the green sheets, and burning out the organic binder, the extruded powder was sintered by SPS as described in Section 2. For comparison, the un-extruded ZnO powder was also sintered by SPS in the same parameters. Fig. 6 shows the displacement of the total height of the samples in the graphite mold during the SPS process. This displacement directly represents the shrinkage profile during densification of the powder in real-time. It can be seen that both kinds of powders started to densify at about 400 °C, the densification rate at low heating rate before 700 °C was lower than that at high heating rate after 700 °C. The densification of both kinds of powders finished at about 900 °C. The density was measured by Archimedes' method. The relative density of both kinds of

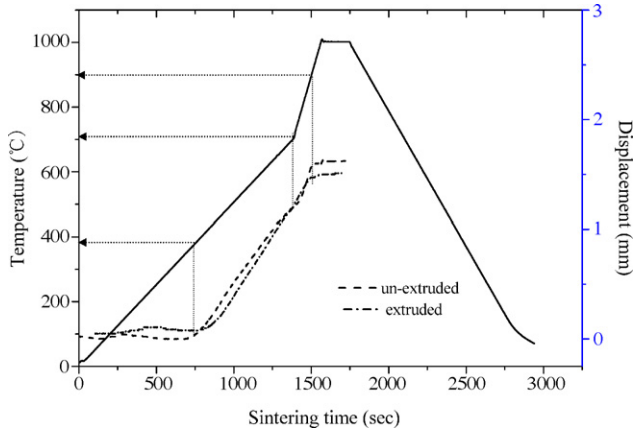

Fig. 6. Shrinkage behavior of the extruded and un-extruded ZnO powder during SPS process.

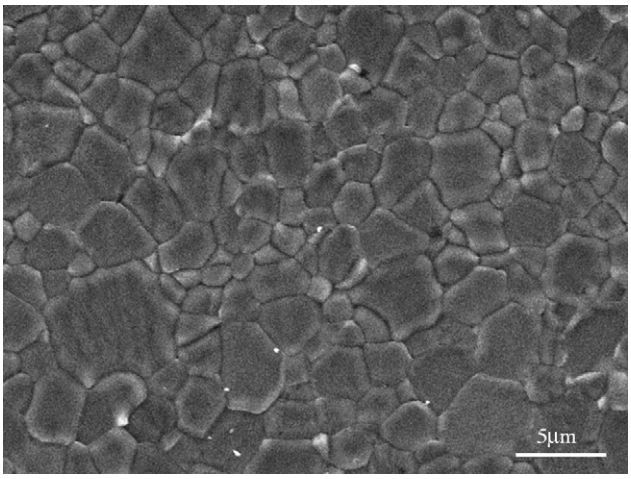

Fig. 7. SEM image from *surface c* of the extruded-SPS ZnO sample.

samples was higher than 99%, which was 99.4 and 99.6% for the extruded- and un-extruded-SPS samples, respectively. These results showed significant improvement compared with a conventional sintering process [24].

Fig. 7 shows the SEM image from *surface c* of the extruded-SPS sample, from which it can be seen that the sintered body was highly densified and pore was invisible. The grains were equiaxial and only several micrometers in size. The image of the un-extruded-SPS sample was similar due to the same SPS process so it is not presented here. Thus, the SPS provides a relative low-temperature, short-time sintering to obtain a near full dense homogeneous microstructure with constrained grain growth using anisotropic particles.

3.3. Grain orientation and grain boundary characteristics

EBSD was utilized to analyze the grain orientation of the extruded-SPS and un-extruded-SPS ZnO samples. Both *surface a* and *surface c* were analyzed. Fig. 8 shows the inverse pole figures of sample normal direction from *surface a* of the un-extruded-SPS and extruded-SPS samples. It can be seen that there is no [0 0 0 1] distribution on both the inverse pole figures, which meant that [0 0 0 1] distributed in a direction parallel to *surface a* but not perpendicular to it. As described above, extrusion can align rod-like particles like this, which has been confirmed by XRD pattern as shown in Fig. 5. However, pressure can also align rod-like particles. When pressure was applied during SPS sintering, the long axis (i.e., [0 0 0 1] direction) of the particle rotated to the direction perpendicular to the pressure. And after SPS, the [0 0 0 1] only distributed in the direction parallel to *surface a*.

Then the *surface c* of both the samples were analyzed using EBSD. Fig. 9 shows the pole figures from *surface c* of the un-extruded-SPS and extruded-SPS samples. From Fig. 9(a), it can be seen that the (0 0 0 1) contour distributed mostly on the vertical bar of the pole figure, which meant that in the un-extruded-SPS sample [0 0 0 1] direction distributed randomly but mostly parallel to a plane which was *surface a*, as described above. Correspondingly, the contours of $(1\,0\,\bar{1}\,0)$ and $(2\,\bar{1}\,\bar{1}\,0)$

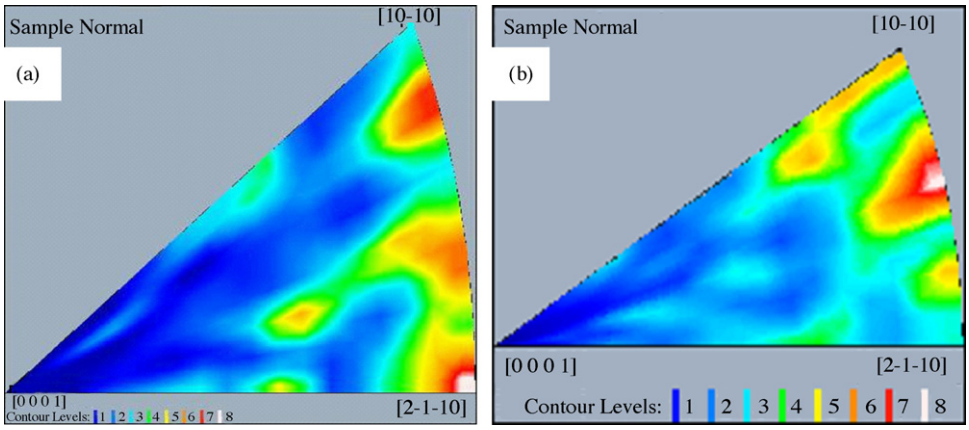

Fig. 8. Inverse pole figures of sample normal direction from *surface a* of (a) un-extruded-SPS sample, and (b) extruded-SPS sample.

distributed almost randomly on their pole figures as shown in Fig. 9(b) and (c), for the $[1\,0\,\bar{1}\,0]$ and $[2\,\bar{1}\,\bar{1}\,0]$ were perpendicular to and surrounded the [0 0 0 1] direction. However, from Fig. 9(d) it can be seen that the [0 0 0 1] direction (i.e., *c*-axis) was highly oriented perpendicularly to *surface c* in the extruded-SPS sample, which meant parallel to the extrusion direction. Correspondingly, the contours of the $(1\,0\,\bar{1}\,0)$ and $(2\,\bar{1}\,\bar{1}\,0)$ were distributed around the edge of their pole figures, which meant that the prismatic planes were aligned in a direction perpendicular to the extrusion direction, as shown in Fig. 9(e) and (f).

Thus, it can be seen that although there was some alignment induced by the pressure in the un-extruded-SPS sample, in which [0 0 0 1] was parallel to and circumrotated in *surface a*, but highly preferred orientation only in one direction (i.e., texture) could not be obtained just by SPS. While the extruded-SPS sample showed a highly *c*-axis preferred orientation in only one direction, which was the extrusion direction. Also, the highly preferred orientation achieved in the extruded-SPS sample can be described as fiber texture, for the texture was controlled only in one particular direction which was *c*-axis direction [25].

By extrusion process, the long axes of the ZnO particles, which were the *c*-axes of the hexagonal crystals, were aligned parallel to the extrusion direction. When SPS process was performed, neck formation and diffusion happened between the particles and the green body started to densify. As the particles had the same alignment direction of [0 0 0 1], when sintering finished, the grains had the same orientation of [0 0 0 1]. Thus, the highly *c*-axis-oriented bulk ZnO was obtained.

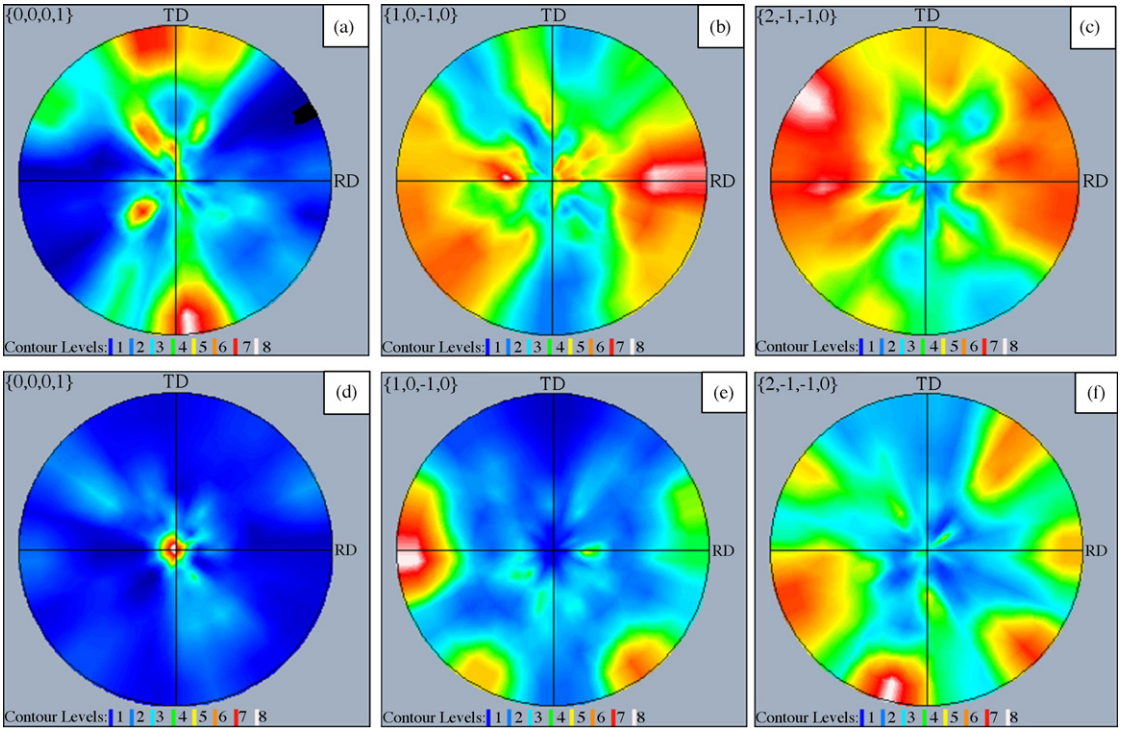

Fig. 9. Pole figures from *surface c*: (a) (0 0 0 1), (b) $(1\,0\,\bar{1}\,0)$ and (c) $(2\,\bar{1}\,\bar{1}\,0)$ pole figures of the un-extruded-SPS sample; (d) (0 0 0 1), (e) $(1\,0\,\bar{1}\,0)$ and (f) $(2\,\bar{1}\,\bar{1}\,0)$ pole figures of the extruded-SPS sample.

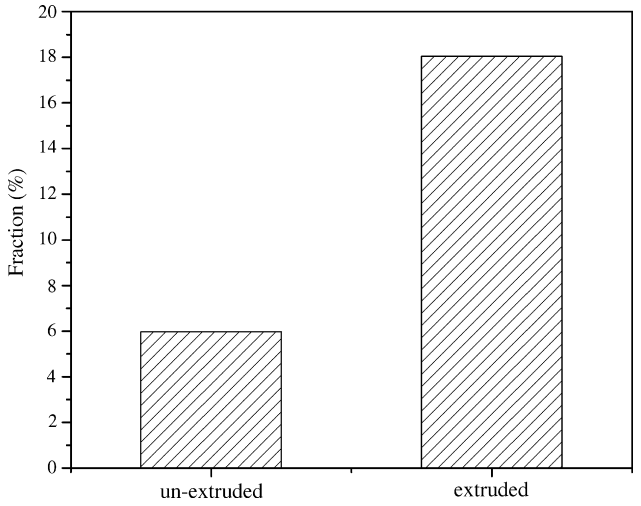

Fig. 10. Statistics for low-angle grain boundaries (misorientation angle $< 15^{\circ}$) from *surface c* of the un-extruded- and extruded-SPS samples.

Further on, the grain boundary characteristics were analyzed by EBSD. Fig. 10 shows the statistics of low-angle grain boundaries (misorientation angle $< 15^{\circ}$) from *surface c* of the un-extruded-SPS and extruded-SPS samples. It can be seen that the extruded-SPS sample with highly preferred orientation exhibited higher proportion of low-angle grain boundaries than the un-extruded-SPS sample. And the total number of the grain boundaries for statistics was about 800 for each sample. The grain boundary characteristics were analyzed on *surface c* in order to correspond with the measurement direction of the electrical properties. The observed higher proportion of low-angle grain boundaries was due to the fact that the extruded-SPS sample had highly preferred orientation, and statistically the probability of observing low-angle grain boundaries was higher [26,27].

3.4. Electrical properties

The electrical properties were measured by impedance spectroscopy to study the influence of texture on the electrical resistivity of bulk ZnO ceramics. The impedance spectrum was measured in the axial direction of the cylindrical sample as shown in Fig. 2(c). So the electric current flew in a direction parallel to *surface c* and went across the grain boundaries which were already measured by EBSD.

It is well known that grain boundaries play an important role in electrical resistivity [3,28,29]. Impedance spectrum can perform an analysis for the electrical properties of grain boundaries and grain interior separately. Fig. 11 shows the impedance spectra of the extruded-SPS sample and the un-extruded-SPS sample at room temperature. The impedance spectra were analyzed with the aid of an equivalent circuit model [3,30–33]. From the impedance spectra, the DC resistivities of the extruded-SPS and un-extruded-SPS samples were obtained, which were 608.36 and $2.45 \times 10^3\ \Omega$ cm, respectively [30]. The reduction in the resistivity of the extruded-SPS sample was due to the highly preferred orientation, which was widely confirmed to decrease electrical resistivity effectively [8,9,14,26].

Both the impedance spectra of the extruded-SPS and un-extruded-SPS samples had two overlapping semicircles which

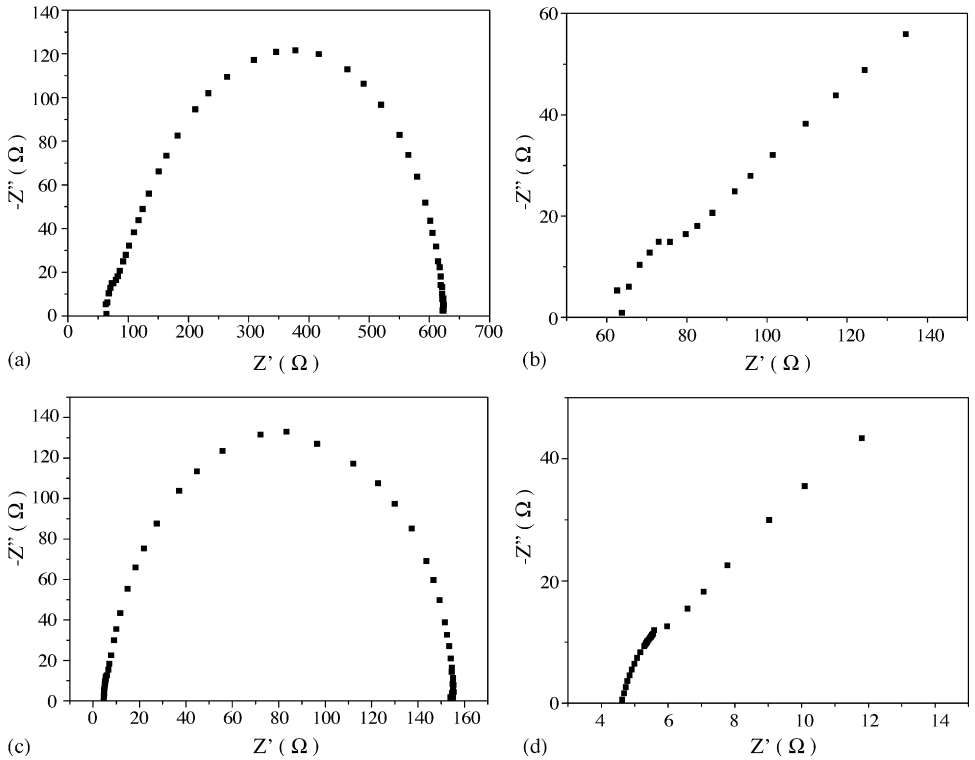

Fig. 11. Impedance spectra of (a) the un-extruded-SPS sample, (b) magnification of (a) in high frequency, (c) the extruded-SPS sample, and (d) magnification of (c) in high frequency.

were not well separated. The large arcs on the right side which were the low frequency parts were the grain boundary arcs, while the small ones on the left side which were the high frequency parts were the grain interior arcs [3,29–32]. Thus, it can be seen that in both extruded and un-extruded cases, the resistivity of grain boundaries was much larger than that of grain interior at room temperature, which meant that grain boundaries played an important role in electrical resistivity. In addition, the grain boundary resistivity of the extruded-SPS sample was much smaller than that of the un-extruded-SPS one, which were 554.6 and $1.92 \times 10^3\ \Omega$ cm, respectively by calculation. This was mainly because of the higher proportion of low-angle grain boundaries in the extruded-SPS sample due to the highly preferred orientation. When misorientation increases, there will be an increase of insulating or normal dislocation core regions in the structure of grain boundaries. This may be caused by the expansion of strain field associated with disordering or disturbance of atomic arrangement with increasing misorientation. And the scattering of electrons by the dislocation core regions will increase the grain boundary resistivity largely in high misorientation boundaries [26,27,34]. In addition, it was reported that there was a trend that the misorientation angles increased with the increase in the size or the amount of the second-phase particles in grain boundaries [34]. Also, it is well known that the second phase or impurities in grain boundaries increase the resistivity. But because the ZnO powder used in this experiment was highly pure and SPS process had a cleaning effect on grain boundaries, so we did not take account of the effect of the impurities in grain boundaries. It was widely confirmed that the low-angle grain boundaries which had misorientation below 15° showed excellent electrical conductivity compared with high-angle grain boundaries [33,35,36]. So the grain boundary resistivity of the extruded-SPS sample was much lower than that of the un-extruded-SPS sample. Also, it can be seen that the lower electrical resistivity of the extruded-SPS sample at room temperature was mainly because of the reduction in the grain boundaries resistivity due to the highly preferred orientation.

4. Conclusion

A textured, near full dense homogeneous bulk ZnO ceramics was prepared successfully using an extrusion-SPS process. Rod-like, anisotropic particles were aligned by the extrusion process. And, after SPS, highly *c*-axis preferred orientation was obtained in the bulk ZnO, which can be called as fiber texture, for it was controlled only in one particular direction. The textured bulk ZnO showed more low-angle grain boundaries compared with that without texture.

Impedance spectroscopy showed that the texture reduced the electrical resistivity of the bulk ZnO obviously at room temperature. It was also shown that the grain boundaries played an important role in electrical resistivity. More proportion of low-angle grain boundaries due to the texture resulted in much lower grain boundary resistivity, which was the main reason for the much lower electrical resistivity of the textured ZnO at room temperature.

These results showed that the extrusion-SPS process was an effective technique to induce texture in bulk ZnO, and the fiber texture was effective in reducing the electrical resistivity of bulk ZnO ceramics.

References

[1] K.F. Cai, E. Miller, C. Drasar, A. Mrotzek, Preparation and thermoelectric properties of Al-doped ZnO ceramics, Mater. Sci. Eng., B 104 (2003) 45–48.
[2] G.K. Paul, S.K. Sen, Sol–gel preparation, characterization and studies on electrical and thermoelectrical properties of gallium doped zinc oxide films, Mater. Lett. 57 (2002) 742–746.
[3] J. Jose, M. Abdul Khadar, Role of grain boundaries on the electrical conductivity of nanophase zinc oxide, Mater. Sci. Eng., A 304–306 (2001) 810–813.
[4] J.W. Zhai, L.Y. Zhang, X. Yao, The dielectric properties and optical propagation loss of c-axis oriented ZnO thin films deposited by sol–gel process, Ceram. Int. 26 (2000) 883–885.
[5] S. Bandyopadhyay, G.K. Paul, R. Roy, S.K. Sen, S. Sen, Study of structural and electrical properties of grain-boundary modified ZnO films prepared by sol–gel technique, Mater. Chem. Phys. 74 (2002) 83–91.
[6] Y. Nakamura, T. Harada, H. Kuribara, Nonlinear, current–voltage characteristics with negative resistance observed at ZnO–ZnO single contacts, J. Am. Ceram. Soc. 82 (11) (1999) 3069–3074.
[7] M. Ohyama, H. Kzuka, T. Yoko, Sol–gel preparation of ZnO films with extremely preferred orientation along (0 0 2) plane from zinc acetate solution, Thin Solid Films 306 (1997) 78–85.
[8] M. Ohyama, H. Kozuka, T. Yoko, Sol–gel preparation of transparent and conductive aluminum-doped zinc oxide films with highly preferential crystal orientation, J. Am. Ceram. Soc. 81 (6) (1998) 1622–1632.
[9] D.H. Bao, H.S. Gu, A.X. Kuang, Sol–gel-derived *c*-axis oriented ZnO thin films, Thin Solid Films 312 (1998) 37–39.
[10] Y. Yoshino, T. Makino, Y. Katayama, T. Hata, Optimization of zinc oxide thin film for surface acoustic wave filters by radio frequency sputtering, Vacuum 59 (2000) 538–545.
[11] T.P. Smith, H. McLean, D.J. Smith, R.F. Davis, Homoepitaxial growth of (0 0 0 1)- and (0 0 0 1)-oriented ZnO thin films via metalorganic vapor-phase epitaxy and their characterization, J. Cryst. Growth, in press.
[12] K.T. Ramakrishna Reddy, T.B.S. Reddy, I. Forbes, R.W. Miles, Highly oriented and conducting ZnO: Ga layers growth by chemical spray pyrolysis, Surf. Coat. Techol. 110–113 (2002) 151–152.
[13] M.H. Aslan, A.Y. Oral, E. Mensur, A. Gul, E. Basaran, Preparation of *c*-axis-oriented zinc-oxide thin films and the study of their microstructure and optical properties, Sol. Energy Mater. Sol. Cells, in press.
[14] T. Schuler, M.A. Aegerter, Optical, electrical and structural properties of sol gel ZnO: Al coatings, Thin Solid Films 351 (1999) 125–131.
[15] S. Isobe, T. Tani, Y. Masuda, W.S. Seo, Thermoelectric performance of yttrium-substituted $(ZnO)_5In_2O_3$ improved through ceramic texturing, Jpn. J. Appl. Phys. 41 (2002) 731–732.
[16] E. Suvaci, İ. Özgür Özer, Processing of textured zinc oxide varistors via templated grain growth, J. Eur. Ceram. Soc., in press.
[17] K. Eda, M. Inada, M. Matsuoka, Grain growth control in ZnO varistors using seed grain, J. Appl. Phys. 54 (2) (1983) 1095–1099.
[18] T.V. Mani, A.D. Damodaran, K.G. Warries, Texture development in BPSCCO superconductors, Am. Ceram. Soc. Bull. 74 (9) (1995) 121–123.
[19] Y. Goto, A. Tsuge, Mechanical properties of unidirectionally oriented SiC-whisker reinforced Si_3N_4 fabricated by extrusion and hot-pressing, J. Am. Ceram. Soc. 76 (6) (1993) 1420–1424.
[20] C.A. Wang, Y. Huang, H.X. Zhai, The effect of whisker orientation in SiC whisker-reinforced Si_3N_4 ceramic matrix composites, J. Eur. Ceram. Soc. 19 (1999) 1903–1909.
[21] L.H. Zou, D.S. Park, B.U. Cho, Y. Huang and H.D. Kim, Characterization of grain alignment in Si_3N_4(w)/Si_3N_4 composites, Mater. Lett., in press.
[22] M. Omori, Sintering, consolidation, reaction and crystal growth by the spark plasma system (SPS), Mater. Sci. Eng., A 287 (2000) 183–188.

[23] Z. Shen, M. Johnson, Z. Zhao, M. Nygren, Spark plasma sintering of alumina, J. Am. Ceram. Soc. 85 (8) (2002) 1921–1927.
[24] M. Takata, D. Tsubone, H. Yanagida, Dependence of electrical conductivity of ZnO on degree of sintering, J. Am. Ceram. Soc. 59 (1–2) (1976) 4–8.
[25] G.L. Messing, Textured Ceramics, Encyclopedia of Materials: Science and Technology, Elsevier Science Ltd., 2001.
[26] Y. Zhu, H. Zhang, H. Wang, M. Suenaga, Grain boundary in textured $Yba_2Cu_3O_{7-\delta}$ superconductor, J. Mater. Res. 6 (12) (1991) 2507–2518.
[27] D. Wolf, S. Yip, Materials Interfaces-atomic-level Structure and Properties, Chapman & Hall, 1992, pp. 191–195.
[28] Y.-M. Chiang, E.B. Lavik, Defect thermodynamics and electrical properties of nanocrystalline oxides: pure and doped CeO_2, Nanostruct. Mater. 9 (1997) 633–642.
[29] J. Jose, M.A. Khadar, Impedance spectroscopic analysis of AC response of nanophase ZnO and ZnO–Al_2O_3 nanocomposites, Nanostruct. Mater. 11 (8) (1999) 1091–1099.
[30] J. Jose, M.A. Khadar, Role of grain boundaries on the electrical properties of ZnO–Ag nanocomposites: an impedance spectroscopic study, Acta Mater. 49 (2001) 729–735.
[31] J. Lee, J.-H. Hwang, J.J. Mashek, T.O. Mason, A.E. Miller, R.W. Sigel, Impedance spectroscopy of grain boundaries in nanophase ZnO, J. Mater. Res. 10 (9) (1995) 2295–2300.
[32] M.H. Abdullan, A.N. Yusoff, Frequency dependence of the complex impedances and dielectric behavior of some Mg–Zn ferrites, J. Mater. Sci. 32 (1997) 5817–5823.
[33] N. Koshizuka, T. Takagi, J.G. Wen, K. Nakao, Critical currents and microstructures of LPE growth YBCO bicrystal films with large single facet grain boundaries, Physica C 337 (2000) 1–6.
[34] K. Ogasawara, N. Sakai, A. Koblischka-Veneva, M.R. Koblischka, Subgrain structures and superconductivity in RE-Ba-Cu-O bulk superconductors, Physica C 386 (2003) 225–230.
[35] A. Goyal, E.D. Specht, Z.L. Wang, D.M. Kroeger, T.A. Mason, D.J. Dingley, Grain boundary misorientation and percolative current paths in high-Jc powder-in-tube (Bi, $Pb)_2Sr_3Ca_3Cu_3O_x$, Appl. Phys. Lett. 66 (21) (1995) 2903–2906.
[36] D. Dimos, P. Chandhari, J. Mannhart, F.K. Legous, Orientation dependence of grain-boundary critical currents in $Yba_2Cu_3O_7$ bicrystals, Phys. Rev. Lett. 61 (1988) 219–222.